Cryoelectron Microscopy of *Escherichia coli* F_1 Adenosinetriphosphatase Decorated with Monoclonal Antibodies to Individual Subunits of the Complex†

Edward P. Gogol, R. Aggeler, M. Sagermann, and Roderick A. Capaldi*
Institute of Molecular Biology, University of Oregon, Eugene, Oregon 97403
Received November 9, 1988; Revised Manuscript Received January 30, 1989

ABSTRACT: Monoclonal antibodies directed against epitopes on each of the five subunits (α, β, γ, δ, and ϵ) of the *Escherichia coli* F_1 ATPase (ECF_1) have been prepared and used to localize the subunits in the enzyme complex. Fab′ fragments, prepared by pepsin digestion of the antibodies, were bound to ECF_1 and visualized by cryoelectron microscopy of the unstained, frozen hydrated ECF_1–Fab′ complexes. Besides aiding in the identification of the ECF_1 subunits, addition of Fab's to the specimen fortuitously offers additional advantages in this technique. ECF_1 labeled with anti-α Fab′ is uniformly oriented in the amorphous ice layer, in contrast to unlabeled ECF_1, which exhibits a multitude of projection views when examined in ice. Almost all complexes display a triangular projection, which image averaging reveals to be a hexagonal view of ECF_1 with Fab′ fragments labeling every other peripheral subunit, confirming the alternating arrangement of α and β subunits in the enzyme. A density in the interior of the structure is positioned asymmetrically, adjacent to an unlabeled peripheral mass, indicating that its primary linkage is to a β rather than an α subunit. The composition of the asymmetric density was explored by examining the trypsin-treated ECF_1, taking advantage of the unique orientation induced by the binding of anti-α Fab′. Trypsin treatment releases the δ and ϵ subunits and cleaves the γ subunit; the internal density is reduced but not eliminated, showing the contribution of the γ subunit to the residual structure, and suggesting that the loss of the δ and ϵ subunits, or a structural rearrangement of the γ subunit, is responsible for its smaller size. Fab′ fragments to accessible epitopes on the γ, δ, and ϵ subunits were localized at the periphery of the hexagonal view of the ECF_1, near the unlabeled β subunits. A wide separation of epitopes on the γ and δ subunits (~40 Å) was demonstrated by simultaneous labeling of ECF_1 with Fab's directed to these sites.

Electron microscopy of F_1 preparations, including negatively stained two-dimensional crystals (Gogol et al., 1989), single particles in negative stain (Tiedge et al., 1983; Akey et al., 1983; Tsuprun et al., 1984; Boekema et al., 1986, 1988), and single molecules embedded in amorphous ice (Gogol et al., 1989), reveals a protein complex made up of seven major densities. Six of these densities are arranged hexagonally around a central cavity, with the seventh density partly occluding this cavity at one end (Gogol et al., 1989). Isolated F_1 is made up of three copies each of the α and β subunits (M_r 55 000 and 50 000, respectively) and one copy each of the γ, δ, and ϵ subunits (M_r 31 000, 19 000, and 15 000, respectively) [reviewed in Senior and Wise (1983), Senior (1988), Vignais and Satre (1984), and Walker et al. (1984)]. Consideration of the sizes and stoichiometries of the subunits suggests that the outer hexagonally arranged densities are the α and β subunits and the central density contains some or all of the three smaller subunits.

Lünsdorf et al. (1984) and Tiedge et al. (1985) used electron microscopy to examine *Escherichia coli* F_1 (ECF_1) and chloroplast F_1, respectively, decorated with monoclonal antibodies against the α subunits. Complexes were observed in negatively stained samples in which the F_1 molecules were associated with one, two, and occasionally three IgG molecules. Antibodies were associated with peripheral densities and spaced by 120° from each other, leading to the conclusion that α and β subunits alternate around the periphery of the F_1 structure. The data obtained in these studies did not unambiguously identify the projection of the F_1 molecule, and the relationship of α and β subunits to the interior mass of smaller subunits was not clear.

We have raised monoclonal antibodies against the subunits of ECF_1 to study structure–function relationships of the enzyme. Here we describe the labeling of ECF_1 with antibodies to the α subunit, using Fab fragments rather than the entire IgG molecules, which were used in previous studies. Unstained specimens were rapidly frozen and examined by cryoelectron microscopy instead of the conventional negative staining technique, to eliminate ionic perturbations and reduce the possibility of physical distortions of the structure. Image averaging of many ECF_1–Fab (anti-α) complexes makes it possible to resolve the antibody fragments distinctly and thus relate the locus of the α subunit to the position of the centrally located seventh mass. Examination of enzyme labeled with anti-α plus anti-γ, -δ, or -ϵ antibodies further defines the position of subunits in ECF_1.

Materials and Methods

ECF_1 from *E. coli* strain AN1460 was isolated and cleaved with trypsin as described by Gavilanes-Ruiz et al. (1988). Trypsin cleavage was carried out in the presence of 0.2% *N*,*N*-dimethyldodecylamine *N*-oxide (LDAO) for 2 h at room temperature at a ECF_1:trypsin ratio of 100:1. The δ subunit was obtained according to Lötscher et al. (1984) from an LDAO-containing sucrose gradient. The γ and ϵ subunits were purified by hydroxyapatite chromatography after dissociation of ECF_1, as described by Dunn and Futai (1980).

Purification of Monoclonal Antibodies. Monoclonal antibodies were raised in the Monoclonal Antibody Facility at the University of Oregon. Cell fusion and growth conditions were as described by Marusich (1988). Mice were injected first with ECF_1 emulsified in Freund's complete adjuvant and

† This work was funded by NIH Grants HL 24526 and GM 39806 to R.A.C.; the electron microscope was obtained with NIH Grant RR 02756.

0006-2960/89/0428-4717$01.50/0

Table I: Cleavage Conditions for Fab′ Production

antibody designation	isotype	yield (mg/L)	pepsin concn (μg/mL)	pH	incubation time (h)
αI	IgG1	29.3	20	3.7	2
αII	IgG1	42.5	75	4.1	19
β_I	IgG1	19.6	20	3.7	3
βII	IgG2a	20.0	75	4.4	7
γI[a]	IgG2b	34.0	2.5	4.4	24
γII	IgG1	65.0	75	4.1	8
γIII	IgG2a	67.7	75	4.4	18
δI	IgG1	33.0	75	4.1	15
εI	IgG1	62.0	75	4.1	20
εII	IgG1	92.0	75	4.1	19

[a] Production of Fab rather than Fab′ fragment due to isotype.

boosted with either 100 μg of ECF_1 or a mixture of the three small subunits, γ, δ, and ε (using 40 μg of each), emulsified in Freund's incomplete adjuvant. Monoclonal antibodies were obtained from hybridomas grown in 1 L of culture media by precipitation with 50% ammonium sulfate at 4 °C. The pellet obtained by centrifugation at 8500 rpm (Sorvall GS3 rotor) for 30 min at 4 °C was washed once with 50% ammonium sulfate, dissolved in 15 mL of phosphate-buffered saline, pH 7.2 (PBS: 137 mM NaCl, 3 mM KCl, 5 mM Na_2HPO_4, and 1.5 mM KH_2PO_4), and dialyzed against two changes of the same buffer. The sample was diluted with an equal volume of the binding buffer of the Affi-Gel protein A monoclonal antibody purification system (MAPSII, Bio-Rad), and antibodies were purified through a protein A–Sepharose column and stored at −20 °C in the elution buffer, adjusted to pH 8–9 by adding 1 M Tris-HCl, pH 9.0.

Formation of NEM-Modified Fab′ Fragments. Fab′–NEM was prepared by cleaving IgG with pepsin to obtain $F(ab')_2$ essentially according to Parham (1983), followed by the reduction of disulfide bridges and reaction with *N*-ethylmaleimide (NEM). Purified immunoglobulins at concentrations between 0.6 and 1.1 mg/mL in PBS were incubated with pepsin, after adjusting the pH to 3.7–4.1 and pH 4.4 for IgG1 and IgG2a, respectively, at 37 °C (Table I). The cleavage was stopped by increasing the pH to 8 with Tris. The $F(ab')_2$ fragments were precipitated with 60% ammonium sulfate, dissolved in PBS, and purified by chromatography on a Sephacryl S200 column (1 × 90 cm) in the same buffer at 4 °C. Fractions containing $F(ab')_2$, as determined by $NaDodSO_4$–polyacrylamide gel electrophoresis, were pooled and, if necessary, purified further through a protein A–Sepharose column, concentrated by ammonium sulfate precipitation or filtration through an Amicon PM 30 membrane, and stored in PBS at −20 °C.

One hundred to two hundred micrograms of $F(ab')_2$ in 200–350 μL of PBS, containing 2 mM EDTA, was reduced with 1–2 mM β-mercaptoethanol for 2 h at room temperature and reacted with 5 mM NEM for 1–2 h. Excess β-mercaptoethanol and NEM were removed by Sephadex G50 chromatography (0.7 × 5 cm) in PBS.

The only antibody of the subclass IgG2b (γI) was directly converted to a Fab fragment by incubation with 2.5 μg/mL pepsin at pH 4.4 for 24 h at 37 °C. Purification was carried out as described for the $F(ab')_2$ fragments.

Assay for the Binding of Monoclonal Antibodies and Fab′ Fragments to ECF_1. Binding of the antibodies and their Fab′ fragments to ECF_1 was determined by ELISA (Goding, 1986). Antigen (ECF_1) was adsorbed to pins in Nunc TSP microwell plates by incubating ECF_1 at a concentration of 10 μg/mL in PBS overnight at 4 °C. The antigen-loaded pins were washed in PBS containing 1 mg/mL bovine serum albumin, 0.05% Triton X-100, and incubated with various amounts of purified IgG or Fab′, for 3 h at room temperature. Following washing with PBS, a secondary antibody, horseradish peroxidase conjugated sheep anti-mouse IgG (Cappel Worthington), in the same buffer was added in a dilution of 1:100, incubated for 1 h at room temperature, and washed with PBS. The pins were then immersed in wells containing the substrate for the enzymatic reaction, 2,2′-azinobis(3-ethylbenzothiazolinesulfonic acid) (diammonium salt, Sigma), at a concentration of 1 mg/mL in 0.1 M sodium citrate at pH 4.0 containing 0.03% H_2O_2. The absorption of each sample was measured at 410 nm.

Electron Microscopy and Image Analysis. ECF_1 (~0.2 mg/mL) was mixed with a 5–10-fold molar excess of NEM-blocked Fab′ fragments and incubated for 1–2 h at room temperature. In order to maximize the binding of Fab′s to the ECF_1, no separation of unbound antibody fragments from the ECF_1–Fab′ complexes was attempted. Aliquots of ECF_1 or the ECF_1–Fab′ mixtures were applied to electron microscope grids covered with holey carbon films, blotted, and rapidly frozen, as described previously (Gogol et al., 1989). Specimens were examined and images recorded (at a magnification of 57000×) as described, with an estimated electron dose of ~20 e^-/A^2, and a defocus of 0.9 μm.

Images were screened visually for the absence of optical artifacts, particularly charge accumulation, and the presence of suitable numbers of particles in thin ice films over holes in the carbon. Areas containing well-separated particles with optimum contrast were digitized as described (Gogol et al., 1989), at a resolution of ~4.4 Å. Individual particles were selected from a graphics display on the basis of clarity, nonoverlap with neighbors, and, in experiments in which ECF_1 was decorated with anti-α Fab′, on the appearance of particles as approximately equilateral triangles; 50–90% of the particles in a scanned area were initially selected for further analysis.

Areas of 32 by 32 pixels were windowed from the scans, approximately centered on the particles, and were aligned by cross-correlation methods, using the SPIDER image analysis program (Frank et al., 1981a,b). The contrast of the particles and their nearly centered position in the windows made low-pass filtration and initial autocorrelation alignment, used in the processing of ECF_1 (Gogol et al., 1989), unnecessary. Well-defined particles were chosen from each data set as initial reference images for alignment. Averages were calculated from subsets of images which aligned most successfully to the initial reference, as judged both by visual methods and by calculated correlation coefficients, and used as references in later rounds of alignment. In the final stages of processing, properly aligned images (usually >80% of the starting images) were classified by the appearance of their central regions. Images within each subcategory were averaged and, where applicable, aligned to one another to generate more inclusive final averages.

Other Methods. Protein concentrations were determined by a modified Lowry procedure (Markwell et al., 1978) for ECF_1, and by measuring the optical density of 280 nm for the antibodies and their fragments $E_{280nm}^{0.1\%,1cm}$ = 1.3–1.5). Samples for $NaDodSO_4$–polyacrylamide gel electrophoresis of immunoglobulin were dissolved in 2% $NaDodSO_4$, 5% glycerol, and 0.12 M Tris (pH 6.8), without reducing agent, and boiled for 3 min; 1.5-mm-thick slab gels were run as described by Laemmli (1970) with a 3% acrylamide stacking gel and an 8% separating gel. Immunoblotting was conducted as described by Gonzalez-Halphen et al. (1988), using sheep anti-mouse IgG conjugated either to horseradish peroxidase

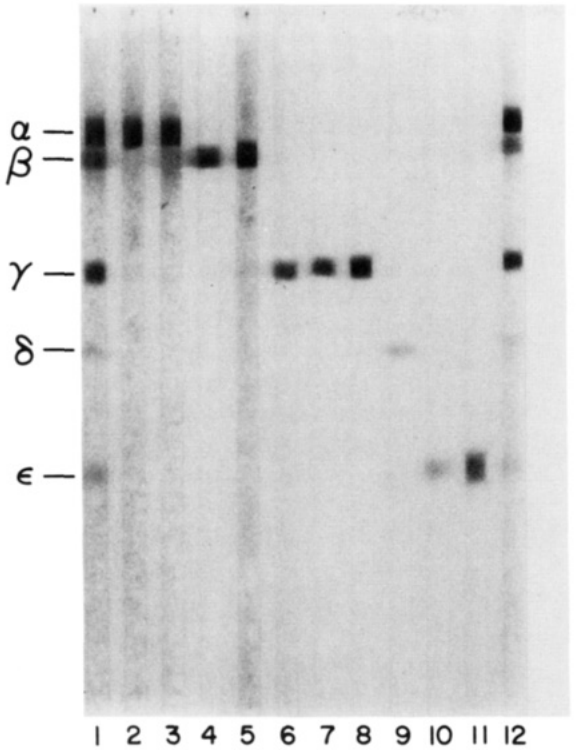

FIGURE 1: Specificity of monoclonal antibodies for individual subunits of ECF_1. 760 μg of ECF_1-ATPase was dissociated in buffer containing 50 mM DTT at room temperature, electrophoresed on a 10–18% polyacrylamide gel, and transferred onto a nitrocellulose membrane for Western blotting. A Miniblotter (Immunetics, Cambridge, MA) was used for the incubation with the monoclonal antibodies (75 μL of each). Lanes 1 and 12, mixture of antibodies against all five ECF_1 subunits; lane 2, 1 μg of αI; lane 3, 1 μg of αII; lane 4, 20 μg of βI; lane 5, 1 μg of βII; lane 6, 10 μg of γI; lane 7, 10 μg of γII; lane 8, 1 μg of γIII; lane 9, 20 μg of δI; lane 10, 20 μg of εI; lane 11, 10 μg of εII.

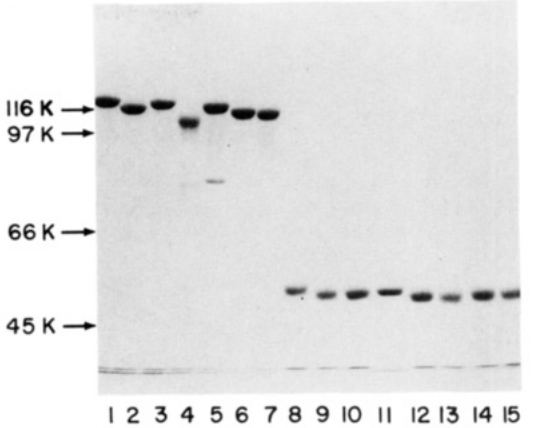

FIGURE 2: $NaDodSO_4$–polyacrylamide gel of $F(ab')_2$ and Fab′ fragments of monoclonal antibodies. Fragments containing the antigen binding site were obtained from purified monoclonal antibodies by cleavage with pepsin (conditions in Table I), reduction with β-mercaptoethanol, and reaction with *N*-ethylmaleimide as described. Unreduced samples (4 μg of each) were run on a $NaDodSO_4$–polyacrylamide gel (8%). The molecular weight markers used were β-galactocidase, phosphorylase B, bovine albumin, and egg albumin from Sigma. $F(ab')_2$ and Fab′ fragments of αI, lanes 1 and 8; αII, lanes 2 and 9; βI, lanes 3 and 10; γII, lanes 4 and 12; δI, lanes 5 and 13; εI, lanes 6 and 14; εII, lanes 7 and 15, respectively; Fab fragment of γI, lane 11.

or to alkaline phosphatase. The subclass of the monoclonal antibodies was determined by using ELISA with the sheep anti-mouse immunoglobulin set (horseradish peroxidase conjugated) from ICN Biomedicals.

Results

Isolation and Characterization of mAbs against Each Subunit of ECF_1. Monoclonal antibodies to the subunits of ECF_1 were obtained from mice injected with the purified native enzyme or with a mixture of the small subunits γ, δ, and ε. Cell lines were screened first for reaction with the native ECF_1 using the ELISA method, and a total of 130 of 4000 lines reacted positively in this analysis. The second phase of screening was by Western blotting to examine reaction with denatured subunits. A total of 56 of the 130 cell lines that were positive in the first screen also reacted with denatured subunits, 10 with α, 5 with β, 28 with γ, 1 with δ, and 12 with the ε subunit. Ten cell lines were picked for subcloning, producing two cell lines secreting antibodies to α, two to β, three to γ, one to δ, and two to ε. The specificity of these mAbs to individual subunits is shown by the Western blot in Figure 1.

Each mAb was purified by protein A–Sepharose column chromatography. The list of antibodies obtained, their subclass, and yields of purified protein from 1 L of culture medium are listed in Table I. $F(ab')_2$ fragments of the monoclonals of the IgG1 type were prepared by using pepsin, as described by Parham (1983), at pHs in the range of 3.7–4.1 with the pH optima and incubation times for the cleavage of each IgG individually determined. $(Fab')_2$ fragments of monoclonals of the IgG2a type were also generated by pepsin cleavage, but at pH 4.4. These $F(ab')_2$ fragments were reduced by mercaptoethanol (1–2 mM) and stabilized as Fab′ by reaction with 5 mM NEM (Figure 2). The antibody of the IgG2b subclass (γI) was converted to Fab rather than Fab′ by cleavage with pepsin.

Binding of intact immunoglobulin and Fab fragment of each monoclonal antibody to ECF_1 was measured by ELISA, and the results are shown in Figure 3. The reactivities of intact IgG and Fab fragments were comparable for four of the mAbs (αI, γI, εI, and εII); in all other cases, the affinity of the Fab for the enzyme was much less than that of the intact IgG.

Electron Microscopy of ECF_1 Fab′ Labeled with Anti-α Fab′. Unlabeled ECF_1 has been visualized in a thin layer of amorphous ice by cryoelectron microscopy, and structural features of the enzyme have been identified by averaging individual images after segregating them into classes of similar projections. Many different orientations of ECF_1 are present in most fields of molecules. Only occasionally, probably in areas where the ice layer (over holes in the grid) is particularly thin, is one orientation favored, resulting in a hexagonal projection (Figure 4A). Even these hexagonal projections can be classified into at least three categories interpretable as slightly different tilts of the molecule around the hexagonal projection (Gogol et al., 1989).

Areas of several electron micrographs of ECF_1, labeled with Fab′(αI), the NEM-reacted Fab′ fragment of the αI mAb, are shown in Figure 4B,C. In areas where the ice thickness varied over the holes, and specimen loading is relatively light, a physical separation of ECF_1–Fab′ complexes from the excess free Fab′ is seen (Figure 4B). In these areas, the ice layer is clearly thinner at the center of the hole, as evident from the lower background density in this region of the micrographs. The small (M_r 55 000) Fab′ fragments segregate to this central region, and they are separated from and surrounded by a halo of well-spaced ECF_1–Fab′ complexes. While exclusion of the ECF_1–Fab′ complexes from the very thin ice at the center of the hole can be understood on the basis of size, their concentration into the surrounding ring is not so readily explained. In cases of higher loading and/or thicker ice, this segregation

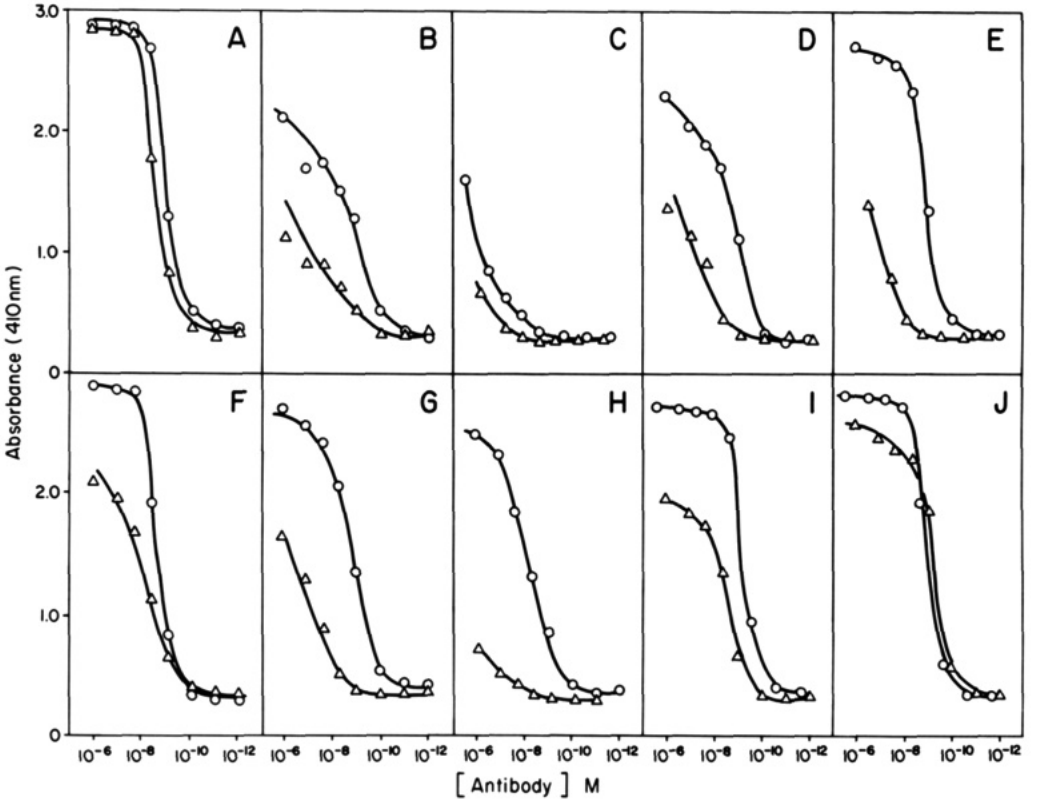

FIGURE 3: Binding of monoclonal antibodies and their Fab′ or Fab fragments to ECF_1. The antibody binding to the ATPase was determined by ELISA assay, with 10 μg/mL ECF_1 and antibody concentrations of 150 μg/mL–0.15 ng/mL. (A) αI; (B) αII; (C) βI; (D) βII; (E) δI; (F) γI; (G) γII; (H) γIII; (I) εI; (J) εII. (○) Entire immunoglobulin; (△) Fab′ fragment (panels A–E and G–J), Fab fragment (panel F).

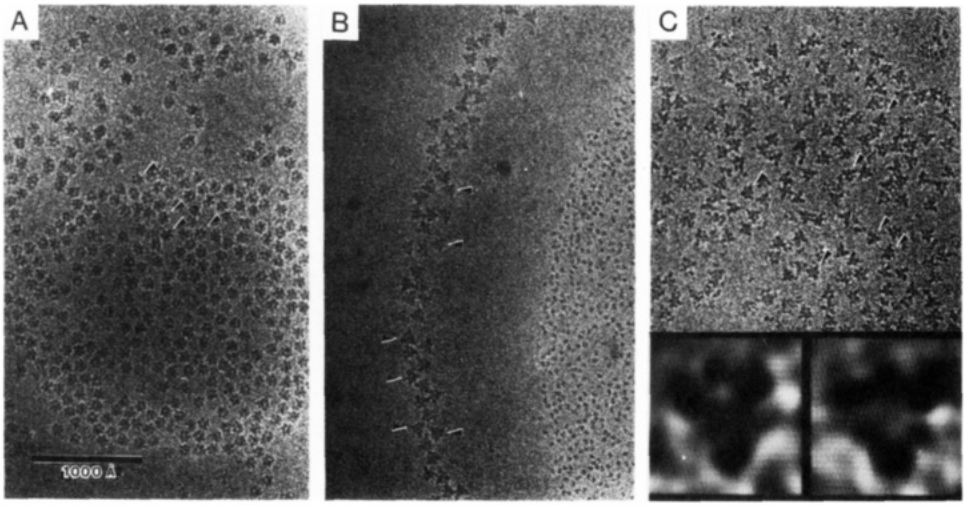

FIGURE 4: Electron micrographs of unstained ECF_1 (A) and ECF_1–Fab′(αI) complexes (B, C) in a thin layer of amorphous ice. Representative hexagonal projections of ECF_1 are indicated by arrows in (A) and by well-separated clear triangular particles in (B). The image in (B) illustrates the clear segregation of ECF_1–Fab′ complexes from free Fab′ (particles on the right) often seen in areas with low specimen density and thin ice; tighter packing of particles is shown in (C). The insets in (C) are magnifications of particles, low-pass-filtered for clarity of display, exhibiting two "hands" of triangle vertices: clockwise on the left, counterclockwise on the right.

was not observed, with ECF_1–Fab′ complexes clustering at the center of holes but often packed too closely for use in single-particle analysis (Figure 4C).

The individual ECF_1–Fab′ complexes have a morphology distinctly different from that of particles of ECF_1 alone: they are equilateral triangles rather than hexagonal structures. Additionally, almost all of the molecules in any field present the same view; the variety of projections seen in electron micrographs of ice-embedded ECF_1 is not present in the Fab′-decorated complexes.

Image Analysis of ECF_1–Anti-α Fab′ Complexes. Views of ECF_1–Fab′ complexes that were well spaced and not overlapped by neighboring particles (such as those in Figure 4B) were selected for image analysis. Close inspection of the individual images of these antigen–antibody complexes confirmed that almost every molecule displayed an equilateral triangular shape, but in two distinct variations, shown in the insets of Figure 4C. These two forms differed in the relative orientation of the protruding vertices of the triangle (Fab′ fragments) and are readily interpretable as particles rotated 180° about an axis normal to the viewing direction. Some fields had both hands of the complex in equal numbers, but most micrographs showed a preponderance of one orientation, possibly induced by the one-sided blotting of the specimen,

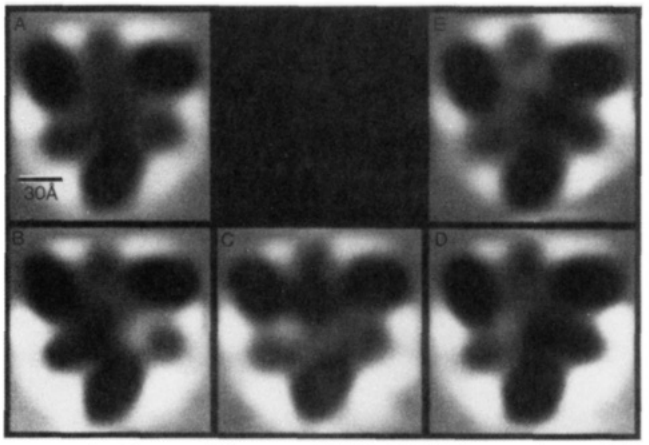

FIGURE 5: Averaged images of ECF_1–Fab′(αI) complexes. (A) Average of 167 images (out of 200 initially selected from 4 micrographs; 33 were rejected for bad alignment or indeterminate handedness) aligned to superimpose the highest contrast features (particularly triangular outline). (B–D) Subcategories of images used to generate (A), sorted by rotational orientation of the internal density, containing 83, 23, and 61 particles, respectively. (E) Final average of panels B–D, weighted by the number of images in each average, after rotating to best superimpose all features. In all of these images, high density (protein) appears dark compared to surrounding ice.

an effect noted in other preparations by Dubochet et al. (1985). Images were all converted to a single hand before further processing.

Most ECF_1–Fab′(αI) images aligned properly to reference images in only a few (two or three) cycles of alignment, as judged by the position and orientation of their triangular outlines. An average of 167 images (out of 200 initially selected ones) is shown in Figure 5A. Close visual inspection of individual images revealed an asymmetric substructure in the central part of the molecule, which was not apparent in this average. These interior features were not superimposed during rotational alignment, presumably because they are of low contrast in comparison to the very dense Fab′-decorated peripheral densities. Most of the images (~80%) could be sorted visually into three categories, on the basis of features at their centers, and averaged (Figure 5B–D). Since they differ only by 120° rotational orientations, these classes were aligned to one another and averaged, after scaling to normalize the number of particles in each, to give the image in Figure 5E. This averaged image shows the interior density located close to one of the peripheral masses, which, since it is not labeled by Fab′(αI), must be a β subunit. The reproducibility of the features of the ECF_1 seen in Figure 5E was demonstrated by analyzing a second data set, collected from images of a different preparation of enzyme, which had been reacted similarly with Fab′(αI) fragments. The two averages were identical, and comparison of the two data sets showed the resolution of each to be ~24 Å, by the criterion of phase residuals below 45° (Frank et al., 1981b).

The averaged image of ECF_1–Fab′(αI) is interpretable as a hexagonal projection of ECF_1 with the densities of three Fab′ fragments superimposed on alternate peripheral subunits. To demonstrate this interpretation, the hexagonal projection of unlabeled ECF_1 (Figure 6A) was scaled to yield peripheral subunit densities equal to those between the vertices of the triangular ECF_1–Fab′ complex (Figure 5E). These two averaged images were then subtracted to produce the difference image shown in Figure 6B, in which the only significant features are the three strong densities of the Fab fragments, arranged in an equilateral triangle with a center-to-center separation of ~70 Å. Other density differences between the

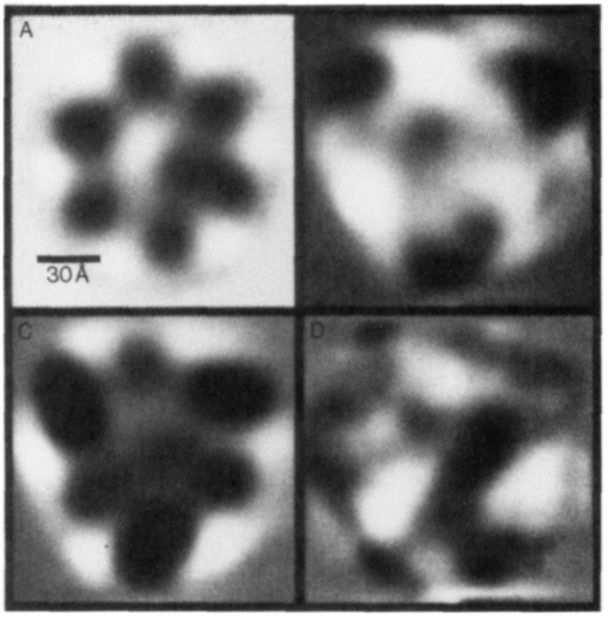

FIGURE 6: Averaged images. (A) Average of ECF_1 images [taken from Gogol et al. (1989)]. (B) Difference image generated by aligning the image in (A) to that in Figure 5E, scaling to equalize unlabeled peripheral densities, and subtracting. (C) Averaged images (133 out of 160 initially selected) of trypsin-cleaved ECF_1 decorated with Fab′(αI), aligned, classified, and averaged as in Figure 5. (D) Difference image generated by subtracting (C) from Figure 5E: the major feature is at the position of the asymmetrically located density at the interior of the view of the molecule in Figure 5E.

two profiles are close to the background. These results show that the α and β subunits alternate around the periphery of the ECF_1.

Labeling of Trypsin-Treated ECF_1 with Anti-α Fab′. ECF_1 treated with trypsin (to cleave γ and remove the δ and ϵ subunits) was also labeled with Fab′(αI) fragments and examined as above. As with native ECF_1, triangular images were observed with the decorated proteolytically modified enzyme (not shown), indicating the binding of three Fab′(αI) to each ECF_1. Averaged images (Figure 6C) generated by the alignment procedure described above reveal the presence of a clearly visible internal density which is, however, significantly reduced in size and more centrally located compared to the native enzyme. This is the major difference between the averages, revealed by the difference image, shown in Figure 6D. The presence of this feature suggests that the γ subunit, even when cleaved, forms the basis of the central structure. A rearrangement of γ and/or a loss of δ and ϵ causes the observed reduction in size.

Labeling of ECF_1 with Anti-γ, Anti-δ, and Anti-ϵ Fab's. The consistent orientation of the ECF_1–Fab′(αI) complexes when embedded in ice provides the opportunity to localize the binding of Fab fragments against other subunits, without the need to classify different views of the complex. Furthermore, the presence of the Fab′(αI) discriminates the α from the otherwise indistinguishable β subunits, making it possible to assess subunit interactions in the ECF_1 complex. Fab fragments against epitopes on the γ, δ, and ϵ subunits could be bound to ECF_1 along with the Fab′(αI) without preventing the formation of the triangular ECF_1–Fab′(αI) complexes, and without affecting the consistent orientation of these particles in the ice layer (Figure 7A). The binding of Fab(γI), Fab′(γII), Fab′(δI), and Fab′(ϵI) could be seen directly by the presence of additional features in some of the triangular particles (e.g., see the arrowed particles in Figure 7A). Free Fab particles, while present in an often large (up to 10-fold)

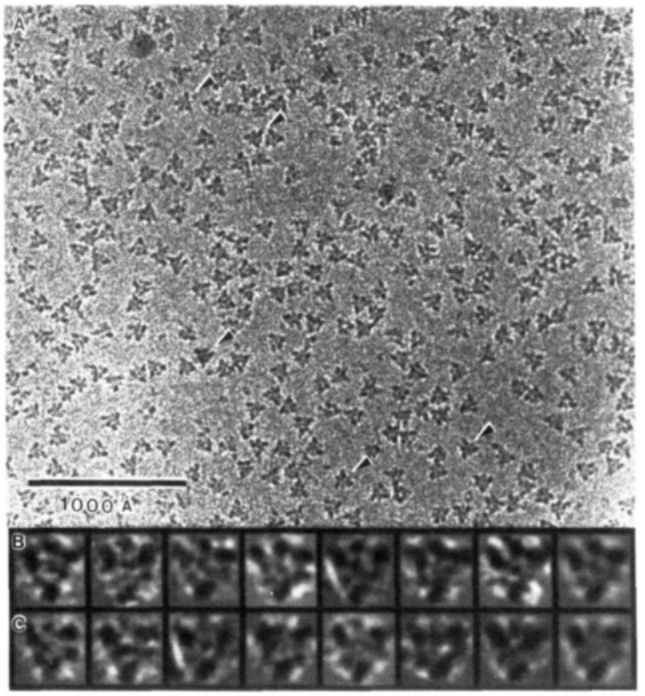

FIGURE 7: (A) Electron micrograph of ECF_1 decorated with both anti-α (αI) and anti-γ (γII) Fab's. Arrows indicate particles which most clearly show an additional density on one side of the triangular particles. (B and C) Galleries of images selected from this micrograph to show the presence and absence, respectively, of the additional density. (The last panel in each gallery is an average of the seven individual images.)

molar excess to ECF_1, were usually only a minor contribution to the visual background, perhaps due to segregation within the ice layer and/or preferential adsorption to the carbon film between holes.

Initially, all of the triangular images of the multiply labeled ECF_1–Fab′ samples were selected, standardized in handedness, aligned against a reference image chosen from the data, and averaged. When an image with an asymmetric peripheral feature (like the arrowed particles in Figure 7A) was chosen as the reference, a similar density appeared in the average of all aligned images, shown in Figure 8A. Alignment of ECF_1–Fab(αI) images (i.e., lacking a second Fab) to the same reference, or to an average like that in Figure 8A, failed to produce a significant increase in density at that position (shown in Figure 8B). Comparison of these averages indicates that the density between the two αI-Fab's at the top of Figure 8A is due to the binding of an additional Fab, in this case Fab(γI). Similar averages are obtained with the other antibody fragments listed above.

The size of the additional feature in these images is smaller than that due to each of the three Fab′(αI) fragments and varies among the different antibodies examined. Visual inspection of the individual images indicated that particles without the peripheral feature were present, in ratios varying from 20% to 50% of the total within any data set. This is not surprising since the concentrations of Fab to the small subunits used in these labeling experiments (at 5–10-fold molar excess of ECF_1) are only near the saturation binding levels. Galleries of particles sorted on the basis of the presence or absence of the fourth Fab are shown in Figure 7B,C. Averages of particles with four Fabs bound show a fourth peripheral density (Figure 8C), averages of the remaining particles (Figure 8D) are nearly 3-fold symmetrical.

In all cases examined to date (γI, γII, δI, ϵI), the fourth antibody fragment is partially superimposed on a β subunit

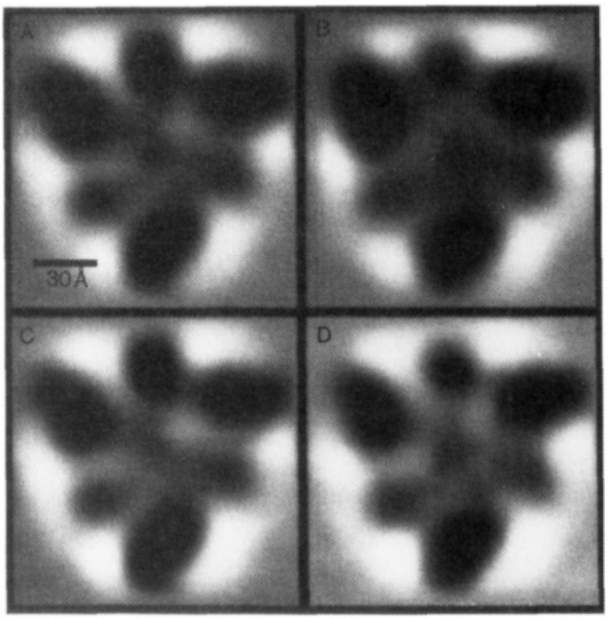

FIGURE 8: (A) Averaged image of ECF_1–Fab′(αI)–Fab(γI), including 176 out of 193 initially selected particles. (The remaining 17 images were rejected due to poor alignment or indeterminate handedness.) (B) Average of 117 images (out of 157 initially chosen) of ECF_1–Fab′(αI), aligned to the average in (A); 40 images were obviously misaligned and thus rejected. Note that the central area of the image, distinctly asymmetric in Figure 5E, is misaligned using this reference. (C) Average of 143 of the 176 images used in (A), selected for the presence of the Fab(γI), i.e., a higher density at the top of the image. (D) Average of the remaining 33 images, which has a reduced density at the top of the image, presumably because most or all of these particles are not labeled by an Fab(γI).

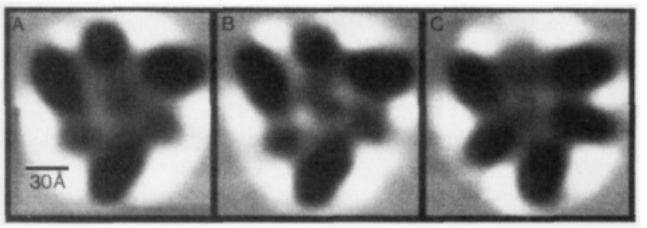

FIGURE 9: Averaged images of multiply labeled ECF_1. (A) ECF_1–Fab′(αI)–Fab′(ϵI). This average includes 55 images; of the 176 initially selected ones, 105 appeared to bind only the 3 Fab′(αI) fragments at the vertices, and the remainder were of poor quality. An average of all the images is similar, but with a less pronounced density at the top of the image. (B) ECF_1–Fab′(αI)–Fab′(γII). This average contains 70 particles out of 153 initially selected; 66 particles appeared to lack the Fab′(γII). (C) Triply labeled ECF_1: ECF_1–Fab′(αI)–Fab(γI)–Fab′(δI). Average of 56 particles; of the 194 initially selected, 86 showed binding of 5 Fab's, 30 of which failed to align or were otherwise of poor quality (an additional 28 images appeared to be decorated with 4 Fab's, and the remainder were triangular).

(e.g., Figures 8C and 9A,B). Even in averages including only particles labeled with the fourth Fab, the density attributed to this fragment appears smaller than that of the Fab′(αI). This difference may be due to orientation of the Fab, or epitope flexibility, which would reduce the density in averages. The additional density of the fourth Fab constrains the rotational alignment of the ECF_1–Fab complex to a single orientation, in contrast to the three orientations of the more symmetrical ECF_1–Fab′(αI). The density of the interior of the ECF_1 appears less contrasted in these doubly labeled molecules than in the ECF_1–Fab′(αI) complexes (compare Figures 8C and 9A or 9B with Figure 5E), making the location of the central mass more difficult to define.

Structural localization of Fab fragments of other antibodies listed in Table I has not been completed. Preliminary ex-

periments indicate that antibodies to the β subunit do not generate the triangular particles seen with Fab'(αI), making image identification, selection, and averaging difficult.

Multiple Labeling of the Small Subunits. Experiments have been conducted in which Fab fragments against α, γ, and δ have been reacted with the ECF_1, yielding a complex with five antibody fragments bound to the enzyme. Figure 9C shows an average of images of the ECF_1–Fab'(αI)–Fab-(γI)–Fab'(δI). The triangular shape due to binding the three anti-α Fab's is obvious, as are two additional densities located near different β subunits. This result shows that the two epitopes, one on γ and one on δ, are spaced wide apart in the hexagonal projection of ECF_1.

Discussion

The topology of several macromolecular assemblies has been studied by localization of polyclonal and/or monoclonal antibody binding sites, using electron microscopy to visualize the antibody–antigen complex [e.g., see Yanagida and Ahmed-Zadeh (1970), Stöffler and Stöffler-Meilicke (1984), Lünsdorf et al. (1984), and Kubalek et al. (1987)]. In most cases, including previous work with F_1, the location of antibody binding sites has been derived from selected single images, limiting the resolution of the structure, and potentially introducing bias by choice of images. Averaging of many images allows identification of reproducible features, along with reduction of background noise. Image averaging is straightforward when the antibody can be used to decorate two-dimensional crystals of the protein [e.g., see Kubalek et al. (1987)], where all the molecules are in the same orientation. However, most proteins do not readily form ordered arrays, and even when crystalline samples can be obtained, antibody accessibility may be limited due to the packing of the molecules. On the other hand, when single particles of the antibody–antigen complex are studied, individual images must be sorted into similar views before they can be averaged.

Our analysis of the topology of subunits in ECF_1 began with experiments using monoclonal antibodies against the α subunit. ECF_1 contains three copies of the α subunit and binds three Fab' fragments against this subunit. Antigen–antibody complexes embedded in a thin layer of ice were visualized by cryoelectron microscopy. The presence of the three Fab' fragments effected a striking change in the size and shape of the enzyme, indicating the presence of the immunolabel more clearly than might be the case in a larger complex. Also fortuitously, almost all of the molecules were oriented in an identical way, exhibiting a hexagonal projection of ECF_1. The uniform orientation of these complexes is in contrast to the many different views seen in most fields of unlabeled ECF_1. Preferred views of particles are commonly seen in specimens adsorbed to a substrate, for example, in negatively stained samples (e.g., the hexagonal view of F_1; Akey et al., 1983; Boekema et al., 1986, 1988). Nonrandom orientations have also been observed in thin unsupported ice films; a preferential adsorption of one surface of the specimen to the air–buffer interface has been postulated to explain this phenomenon (Dubochet et al., 1988). This interaction, while sometimes determining the orientation of molecules in solution, is a much weaker physical perturbation than adsorption onto a solid hydrophilic surface; the latter force is dominant in ice films over carbon, as well as in negatively stained specimens.

This consistent orientation of ECF_1–Fab'(αI) complexes allowed the averaging of images of most of the particles in a field of view, without the need for subjective selection and extensive classification. Our only criterion for initial particle selection was nonoverlap with neighboring molecules. Since most (>90%) of the images were equilateral triangles in outline, this additional standard was applied to the choice of aligned particles to average. In other experiments, ECF_1 was decorated with combinations of the anti-α plus anti-γ, anti-δ, or anti-ϵ subunit antibody fragments. ECF_1 which had been cleaved with trypsin was also decorated with anti-α Fab', allowing a direct comparison of the native and proteolytically modified structures. In all cases, particles were chosen on the basis of the above criteria: the presence of any additional features was ignored in image selection.

Averages of the images of the ECF_1–Fab'(αI) complexes confirm features of the hexagonal view of ECF_1 seen previously (Gogol et al., 1989): there are six peripheral densities surrounding a central cavity, which contains an interior protein density associated with one of the six outer ones. The labeling studies add detail to this picture. Fab'(αI) fragments were found to superimpose on every second density around the periphery, demonstrating the alternating arrangement of α and β subunits in the enzyme. The more centrally located density is proximal to one of the unlabeled peripheral densities, identified as a β subunit.

The first insights into the composition of the interior density were obtained by examining the effects of trypsin on ECF_1. Under the condition of our experiments, trypsin completely removes the δ and ϵ subunits, cleaves away the N-terminal 15 residues of the α subunit and a small fragment from the C terminus of the β subunit, and separates the γ subunit into two domains each of which remains associated with the ECF_1, but with the release of a small peptide in the vicinity of residue 200 (Gavilanes-Ruiz et al., 1988). This treatment does not inactivate the enzyme; on the contrary, there is up to a 10-fold increase in ATPase activity, partly as a result of the release of ϵ from the ECF_1. Images of the trypsin-treated enzyme reveal the presence of a central density which has been reduced in size. This residual structure must therefore consist of either the N-terminus (residues 1 to approximately 195), C-terminus (residues 202–287), or both parts of the cleaved γ subunit, with the observed reduction in size due to a rearrangement of the γ subunit and/or to loss of δ and ϵ subunits. Its more symmetrical location is likewise due to this rearrangement or loss and/or to the cleavage of the C-terminus of the β subunit.

Genetic studies have established the critical role of the γ subunit in the assembly of the ECF_1 complex (Miki et al., 1986). Mutations in either the N- or the C-terminus prevent association of α and β subunits to form the active enzyme. Both N- and C-terminal parts of γ contain highly conserved sequences; the central region near the typsin cleavage site in ECF_1 [and CF_1; see Schumann et al. (1985)] has significant interspecies variability. One of the anti-γ mAb's used in this study (γII in Figures 1 and 3) is directed against an epitope in the C-terminal third of the sequence; another (γI) interacts with the peptide which can be removed by trypsin cleavage, the interdomain linking region around residue 200 (Aggeler et al., unpublished results). When bound to ECF_1, Fab' fragments of both of these antibodies are located at the periphery of the complex, near β subunits (shown in Figures 8C and 9B), suggesting that it is the larger N-terminal domain of γ which is at the interior of the ECF_1. Fab's directed to the δ and ϵ subunits (δI and ϵI) also appear to be localized to the periphery of the ECF_1, suggesting that, if either subunit is part of the central density, it has extended regions which include the epitopes for these two antibodies.

Averaged images of ECF_1 labeled with anti-γ, -δ, or -ϵ Fab's along with Fab'(αI) have a diffuse internal density which appears to be somewhat delocalized. A preliminary analysis

of the individual images with the clearest internal features suggests that the central density is similar in appearance to that in ECF_1–Fab′(αI) complexes. However, the loci of the antibody epitopes on the small subunits are not fixed with respect to the internal structure, but rather vary among three locations (related by 120° rotations). These epitopes, located on the C-terminal domain of the γ and unidentified parts of the δ and ϵ subunits, therefore appear to be localized independently of the central density, whose core, as discussed above, probably consists of the N-terminal domain of the γ subunit. Confirmation of this observation will require the analysis of a much larger data set than presently available. Such results would support models of the enzymatic mechanism which postulate a movement of small subunits or parts of them with respect to one another as well as to the peripheral α and β subunits.

ACKNOWLEDGMENTS

We thank Dr. Marina Gavilanes-Ruiz for preparation of the trypsin-treated ECF_1, Dr. Michael Marusich and Beth Prescott for raising the monoclonal cell lines, and Dr. Brian Matthews for use of computer facilities.

Registry No. ATPase, 9000-83-3.

REFERENCES

Akey, C. W., Crepeau, R. H., Dunn, S. D., McCarty, R. E., & Edelstein, S. J. (1983) *EMBO J. 2*, 1409–1415.

Boekema, E. J., Berden, J. A., & van Heel, M. G. (1986) *Biochim. Biophys. Acta 851*, 353–360.

Boekema, E. J., van Heel, M., & Gräber, P. (1988) *Biochim. Biophys. Acta 933*, 365–371.

Dubochet, J., Adrian, M., Lepault, J., & McDowall, A. W. (1985) *Trends Biochem. Sci. 10*, 143–146.

Dubochet, J., Adrian, M., Chang, J.-J., Homo, J.-C., Lepault, J., McDowall, A., & Schultz, P. (1988) *Q. Rev. Biophys. 21*, 129–228.

Frank, J., Shimkin, B., & Dowse, H. (1981a) *Ultramicroscopy 6*, 343–358.

Frank, J., Verschoor, A., & Boublik, M. (1981b) *Science 214*, 1353–1355.

Gavilanes-Ruiz, M., Tommasino, M., & Capaldi, R. A. (1989) *Biochemistry 27*, 603–609.

Goding, J. W. (1986) *Monoclonal Antibodies: Principles and Practice*, Academic Press, London.

Gogol, E. P., Lücken, U., Bork, T., & Capaldi, R. A. (1989) *Biochemistry* (preceding paper in this issue).

Gonzales-Halphen, D., Lindorfer, M. A., & Capaldi, R. A. (1988) *Biochemistry 27*, 7021–7031.

Kubalek, E., Ralston, S., Lindstrom, J., & Unwin, N. (1987) *J. Cell Biol. 105*, 9–18.

Laemmli, U. K. (1970) *Nature (London) 227*, 680–685.

Lötscher, H. R., deJong, C., & Capaldi, R. A. (1984) *Biochemistry 23*, 4134–4140.

Lündsdorf, H., Ehrig, K., Friedl, P., & Schairer, H. U. (1984) *J. Mol. Biol. 173*, 131–136.

Markwell, M. A. K., Haas, S. M., Bieber, L. L., & Tolbert, N. E. (1978) *Anal. Biochem. 87*, 206–210.

Marusich, M. (1988) *J. Immunol. Methods 114*, 155–159.

Miki, J., Takeyama, M., Moumi, T., Kanazana, H., Maeda, M., & Futai, M. (1986) *Arch. Biochem. Biophys. 251*, 458–464.

Parham, P. (1983) *J. Immunol. 131*, 2895–2902.

Schumann, J., Richter, M. L., & McCarty, R. E. (1985) *J. Biol. Chem. 260*, 11817–11823.

Senior, A. E. (1988) *Physiol. Rev. 68*, 177–231.

Senior, A. E., & Wise, J. G. (1983) *J. Mol. Biol. 73*, 105–124.

Stöffler, G., & Stöffler-Meilicke, M. (1984) *Annu. Rev. Biophys. Bioeng. 13*, 303–330.

Tiedge, H., Lünsdorf, H., Schäfer, G., & Mayer, F. (1983) *Eur. J. Biochem. 132*, 37–45.

Tiedge, H., Lünsdorf, H., Schäfer, G., & Schairer, H. V. (1985) *Proc. Natl. Acad. Sci. U.S.A. 82*, 7874–7878.

Tsuprun, V. L., Mesyanzhinova, I. V., Kozlov, I. A., & Orlova, E. V. (1984) *FEBS Lett. 167*, 285–290.

Vignais, P. V., & Satre, M. (1984) *Mol. Cell. Biochem. 60*, 33–70.

Walker, J. E., Saraste, M., & Gay, N. J. (1984) *Biochim. Biophys. Acta 768*, 164–200.

Yanagida, M., & Ahmad-Zadeh, C. (1970) *J. Mol. Biol. 51*, 411–421.